PFC/JA-85-35

Theory of Harmonic Gyrotwystron

T.M. Tran[a], K.E. Kreischer and R.J. Temkin

Plasma Fusion Center
Massachusetts Institute of Technology
Cambridge, MA 02139

October 1985

This work was supported by the U.S. Department of Energy Contract No. DE-AC02-78ET51013.

[a] Permanent address: CRPP, Association Euratom-Confédération Suisse, EPFL, 21, Av. des Bains, CH-1007 Lausanne, Switzerland

Theory of Harmonic Gyrotwystron

T.M. Tran[a)], K.E. Kreischer and R.J. Temkin.

Plasma Fusion Center

Massachusetts Institute of Technology

Cambridge, MA 02139

ABSTRACT

In this paper, the energy extraction stage of the gyrotwystron is investigated by using a self consistent rf field model. In the low field, low current limit, expressions for the self consistent field and the resulting energy extraction efficiency are derived analytically for an arbitrary cyclotron harmonic number. To our knowledge, these are the first analytic results for the self consistent field structure and efficiency of a gyrotron device. The large signal regime analysis is carried out by numerically integrating the coupled self consistent equations. Several examples in this regime are presented.

[a)] Permanent address: CRPP, Association Euratom-Confédération Suisse, EPFL, 21, Av. des Bains, CH-1007 Lausanne, Switzerland

I. INTRODUCTION

In the gyroklystron[1], the electrons entering the energy extraction resonator are previously bunched in their phase angles by the buncher stage. As a result, high efficiency can be expected. Stable single mode emission is anticipated because the beam current can be lower than the threshold current for parasitic mode excitation in the output resonator. Important applications include rf driven accelerators[2], radars[3] besides the obvious application in rf heating of fusion plasmas.

The gyrotwystron[4] can be regarded as a gyroklystron in which the energy extraction stage consists of a travelling wave section. Compared to the gyroklystron, its main characteristic is the quasi-absence of a wave reflection by the cavity, resulting in a minimum cavity Q. The feedback is thus provided by the presence of the electrons in the cavity.

In general, two different theoretical models are employed to describe the rf field-electron interaction in the energy extraction resonator. The first model [1-2,4-6], which is the simplest one, assumes that a rf field spatial profile can be prescribed (usually a Sine or a Gaussian function for the axial field distribution) independently of the electron beam current. This model can somehow be improved by including the effect of the electron current on the wave frequency[2]. In a previous paper[7], we have adopted this simple approach in order to examine the optimum operation in gyroklystrons in terms of a minimum number of normalized parameters.

The second model treats the rf field-electron interaction self consistently and has extensively been used in the analysis of single cavity gyrotron[8-9] where the electrons are not prebunched. This approach is proven to be more appropriate than the first model for low-Q resonators. For multiple cavity gyroklystrons, a small signal theory based on this approach has been given in refs.10 and 11.

In the present work, we adopt the self consistent approach to investigate both the low field, low current regime and the large signal regime in the energy extraction resonator of a gyrotwystron. The basic model is briefly reviewed in section II. In section III, a comprehensive analytical study is presented in the low field, low current regime, assuming a simple expression for the bunched electron distribution at the entrance of the energy extraction resonator. Analytical expressions for the self consistent field profile as well as the energy extraction efficiency are obtained for all cyclotron harmonics; these results may also serve as a useful test for nonlinear self consistent numerical codes. Section IV describes a numerical procedure to solve the self consistent equations, based on the finite element method. Applications of this method are illustrated for the case of the gyrotwystron in the low current regime as well as in the high current regime. Comparison with the results obtained from the simple fixed field model is also examined. Finally, the conclusions of the present work will be outlined in section V.

II. PHYSICAL MODEL AND ASSUMPTIONS

II.A Basic Equations

In the present analysis, we consider an annular beam of magnetized weakly relativistic electrons interacting with the transverse electric (TE) field

$$\mathbf{E}_t(r,\varphi,z,t) = E_o \frac{f(z)}{k_\perp(z)} \hat{e}_{mp}(r,\varphi,z,t) \tag{1}$$

where $\hat{e}_{mp}$ denotes the familiar TE_{mp} eigenmode in a cylindrical resonator

$$\hat{e}_{mp} = \left[imJ_m(k_\perp r)\hat{e}_r/r + k_\perp J'_m(k_\perp r)\hat{e}_\varphi \right] e^{i(\omega t - m\varphi)}.$$

The transverse wave number $k_\perp = \nu_{mp}/R$ (ν_{mp} and R are respectively the p^{th} nonzero root of J'_m and the cavity radius) is a slowly varying function of the z coordinate. The dimensionless function $f(z)$ in Eq.(1) describes the spatial profile of the rf field and is normalized to its maximum value. Throughout the analysis, we assume that

a. only one mode is present in the resonator

b. the interaction occurs near the cut-off frequency of the resonator ($k_{||} \ll k_\perp$)

c. the collective effects are negligible

Within the assumptions mentioned above, the electron dynamics can be described by a slow time scale model where the fast cyclotron motion is averaged out. By choosing an appropriate normalization, the single particle, single mode equations for the electron motion at the n^{th} cyclotron harmonics can be reduced to the well-known first order differential equation for the complex momentum P (see for example refs.8,9):

$$\frac{dP}{d\varsigma} + i(\Delta - 1 + w)P = -inFf(\varsigma)w^{n-1} \tag{2}$$

with the following definitions:

$$P = \left(\frac{\gamma\beta_\perp}{\gamma_o\beta_{\perp o}}\right)^n \exp(i\theta) \tag{3.a}$$

$$w = |P|^{\frac{2}{n}} \tag{3.b}$$

$$\varsigma = \frac{\beta_{\perp o}^2}{2\beta_{\|o}} kz \tag{3.c}$$

$$\Delta = \frac{2}{\beta_{\perp o}^2}\left(1 - \frac{n\omega_{co}}{\omega}\right) \tag{3.d}$$

$$F = \frac{E_o\beta_{\perp o}^{n-4}}{Bc}\left(\frac{n^{n-1}}{2^{n-1}n!}\right) J_{m\pm n}(k_\perp R_e) \tag{3.e}$$

In these equations, the subscript o designates quantities defined at the entrance of the resonator, $\beta_\perp = v_\perp/c$, $\beta_{\|} = v_{\|}/c$ are respectively the transverse and the parallel velocities normalized to the light velocity c, γ is the relativistic factor, ω_{co} is the relativistic cyclotron frequency, B is the static magnetic field and R_e is the electron beam radial position. In addition, an appropriate transverse momentum distribution for the bunched electrons at the entrance of the resonator (depending on the chosen model for the prebuncher) should be given to specify the required initial condition for the differential equation (2).

Using the expression for the rf field given in Eq.(1) and the Maxwell equations, one can obtain[9] the equation for the field profile function f:

$$\left[\frac{d^2}{dz^2} + (k^2 - k_\perp^2)\right]\left(\frac{f}{k_\perp}\right) = -k_\perp\left(\frac{\beta_{\perp o}^2}{2\beta_{\|o}}\right)^2 \frac{I}{F}\langle P\rangle \tag{4}$$

where a weakly wall tapered resonator has been assumed. In the rhs of Eq.(4), I designates a dimensionless current proportional to the beam current I_A (in Amp.) as defined by

$$I = \frac{16}{\pi}\frac{eI_A}{\epsilon_o m_e\gamma_o c^3}\beta_{\perp o}^{2(n-4)}\beta_{\|o}\left(\frac{n^n}{2^n n!}\right)^2 \frac{J_{m\pm n}^2(k_\perp R_e)}{(\nu_{mp}^2 - m^2)J_m^2(\nu_{mp})} \tag{5}$$

and $\langle\cdots\rangle$ defines an ensemble average over the electrons. Assuming a negligible field amplitude in a cutoff section at the entrance of the resonator ($z = z_{in}$) and the radiation

condition at the resonator output ($z = z_{out}$), the appropriate boundary conditions for Eq.(4) can be formulated as

$$\left[\frac{f}{k_\perp}\right]_{z=z_{in}} = 0 \tag{6.a}$$

$$\left[\frac{d}{dz}\frac{f}{k_\perp}\right]_{z=z_{out}} = -i\left[k_\parallel \frac{f}{k_\perp}\right]_{z=z_{out}} \tag{6.b}$$

II.B Conservation Relations

Multiplying Eq.(4) by $f^*/k_\perp$ and integrating from z_{in} to z_{out} yield

$$2k\left[k_\parallel \left|f/k_\perp\right|^2\right]_{z=z_{out}} = \frac{\beta_{\perp o}^2}{2\beta_{\parallel o}} I\chi_i \tag{7.a}$$

$$2k\int_{z_{in}}^{z_{out}} \left[\left|d/dz\,(f/k_\perp)\right|^2 - \left|k_\parallel f/k_\perp\right|^2\right] dz = \frac{\beta_{\perp o}^2}{2\beta_{\parallel o}} I\chi_r \tag{7.b}$$

where we have introduced the complex coupling term defined as

$$\chi = \chi_r + i\chi_i = \frac{2}{F}\left(\frac{2\beta_{\parallel o}}{\beta_{\perp o}^2}k\right)\int_{z_{in}}^{z_{out}} f^*\langle P\rangle\, dz = \frac{2}{F}\int_{\zeta_{in}}^{\zeta_{out}} f^*\langle P\rangle\, d\zeta \tag{8}$$

On the other hand, it can easily be shown from Eq.(2) that the transverse energy conversion efficiency $\eta_\perp = 1 - \langle w(z_{out})\rangle$ is related to χ by

$$\eta_\perp = F^2\chi_i \tag{9}$$

Therefore, the relation (7.a) states that the power emitted by the electron beam is balanced by the rf power diffracted through the output section of the resonator. The second relation (7.b) describes the frequency shift due to the presence of the electron beam. It is interesting to note that the same conservation relations can be derived from the time-dependent wave equation (assuming for example a fixed, Gaussian rf field profile) and the conditions for equilibrium[6].

In high-Q resonators where the rf field profile $f(z)$ can be approximated by an empty cavity eigenmode (obtained by solving Eq.(4) with $I = 0$), these relations can be used to determine the steady state output power as well as the oscillation frequency, once χ is known from numerically integrating the electron equation of motion with a given field magnitude F. For low-Q resonators, the rf field profile equation (4) should be calculated self consistently with the electron equation of motion (2); the relations (7) then can serve as an useful diagnostic for the numerical procedure.

III. LINEAR ANALYSIS

In this section we want to derive analytically the efficiency in the small signal regime from the self consistent gyrotron equations given in Eqs.(2) and (4). For the sake of simplicity, we assume that the electrons emerging from the buncher stage are monoenergetic and have a phase angle distribution given by[7]

$$\theta(\varsigma = 0) = \theta_o + q \sin\theta_o - \theta_d, \qquad \theta_o \text{ uniformly distributed over } [0, 2\pi] \tag{10}$$

where q is a dimensionless bunching parameter and θ_d is a constant free-streaming term. In addition, we assume that the gyrotwystron output section has a constant radius ($k_\perp$ = const.) and a constant magnetic field (Δ = const.) along the z-axis. The interaction region is characterized by an effective length μ (normalized accordind to Eq.(3.c)) which can be defined either by changing abruptly the magnetic field or by introducing a weak irregularity on the cavity wall radius, at some position in the travelling wave tube. The wave equation (4) can then be written in the following dimensionless form

$$\begin{aligned} \frac{d^2 f}{d\varsigma^2} + \kappa^2 f &= -\frac{I}{F}\langle P \rangle \\ \kappa^2 &= \left(\frac{2\beta_{\|o}}{\beta_{\perp o}^2}\right)^2 \left(1 - \frac{k^2}{k_\perp^2}\right) \end{aligned} \tag{11}$$

In the limit of small F, Eq.(2) together with the initial condition specified by Eq.(10) can be readily solved to the first order in F. Then, by averaging P over the initial electron phase angle distribution, one obtains the following expression

$$\begin{aligned} \frac{\langle P(\varsigma)\rangle}{F} = -e^{-i\Psi(\varsigma)} \Bigg\{ \frac{J_1(q)}{F} e^{-i\theta_d} + \int_0^\varsigma d\varsigma' \int_0^{\varsigma'} d\varsigma'' \left[f e^{i\Psi(\varsigma'')} - J_2(2q) e^{-2i\theta_d} f^* e^{-i\Psi(\varsigma'')} \right] \\ + in \int_0^\varsigma d\varsigma' f e^{i\Psi(\varsigma')} \Bigg\} \end{aligned} \tag{12}$$

$$\Psi(\varsigma) = \int_0^\varsigma \Delta \, d\varsigma'$$

The first term in the rhs of Eq.(12) designates the unperturbed prebunched electron current. For low current I and optimum prebunching ($q \simeq 2$), the contribution from this term is dominant and a straightforward integration of Eq.(11) yields to the lowest order in I

$$f(\varsigma) = \frac{I}{F} J_1(q) e^{-i\theta_d} \frac{e^{-i\Delta\varsigma}}{\kappa + \Delta} \left\{ \frac{1 - e^{-i(\kappa-\Delta)\varsigma}}{\kappa - \Delta} - i \frac{\sin \kappa\varsigma}{\kappa} e^{-i\kappa\mu} e^{i\Delta(\varsigma-\mu)} \right\} \tag{13}$$

The complex coupling term χ defined by Eq.(8) can then be calculated and finally, employing the definition of the transverse efficiency in Eq.(9) yields

$$\eta_\perp = I\mu^3 J_1^2(q) G(\kappa\mu, \Delta\mu)$$

$$G(x,y) = \frac{2}{x+y} \left\{ \frac{1-\cos(x-y)}{(x-y)^2} + \frac{1}{2x} \left[\frac{\cos 2x - \cos(x+y)}{x-y} + \frac{1-\cos(x-y)}{x+y} \right] \right\} \tag{14}$$

One can note that the dimensionless parameters $x = \kappa\mu$ and $y = \Delta\mu$ can be written in terms of the physical quantities as

$$\begin{aligned} x &= k_{\|} L = \left(\omega^2 - \nu_{mp}^2/R^2\right)^{\frac{1}{2}} L/c \\ y &= (\omega - n\omega_{co})\, L/v_{\|o} \end{aligned} \tag{15}$$

The function G, shown in Fig.(1), exhibits several maxima corresponding to the different longitudinal modes that can be excited in the cavity. The first maximum occurs at $\Delta = 0$, $k_{\|} L = 1.69 \simeq \pi/2$ and is equal to $0.519 \simeq 16/\pi^3$.

By comparing these results with those derived from the gyroklystron model[7] in which the resonator is characterized by a minimum $Q \simeq 4\pi L^2/\lambda^2$ and a Gaussian field profile, one can note that the dependence of the efficiency $\eta_\perp$ on I, μ, q is the same for both models, although the rf field profile in the gyrotwystron, given in Eq.(13), is not Gaussian. Moreover, the optimum $\eta_\perp$ occurs at $\Delta = 0$, $q = 1.84$ in both models and has the same value, provided that the width of the Gaussian is sligthly smaller than the gyrotwystron length, $\mu_{Gaussian} \simeq 0.87\, \mu_{GTW}$.

The bandwidth can be estimated from Eq.(15) and Fig.(1) as

$$\left(\frac{\delta\omega}{\omega}\right)_{(-1dB)} \simeq \frac{1}{8\pi^2} \left(\frac{\lambda}{L}\right)^2 \delta x^2 = 0.07 \left(\frac{\lambda}{L}\right)^2 \tag{16}$$

This relation shows that the bandwidth is only a function of the interaction length L/λ. The same bandwidth dependence is found in the fixed field model since the bandwidth, in that model, is inversely proportional to Q which goes as L^2/λ^2. It should be pointed out here, that the simple small signal results obtained above are applicable for any cyclotron harmonic n.

IV. NONLINEAR ANALYSIS

This section presents a numerical procedure to solve iteratively the self consistent single mode equations (2) and (4) which describe the steady state in the gyrotwystron output resonator. The frequency of oscillation ω in this resonator is fixed by the operating conditions at the buncher stage and is then considered as a known parameter in our analysis. At the entrance of the resonator we assume that the electrons are monoenergetic and have an initial phase angle distribution characterized by only one parameter q as specified by Eq.(10) [the constant term θ_d can be dropped by the substitutions $P \rightarrow Pe^{i\theta_d}$, $f \rightarrow fe^{i\theta_d}$ in Eqs.(2,4)]. However, more realistic initial distributions can be easily implemented in the present procedure.

By choosing a convenient normalization defined by $\bar{R} = R/R_N$, $\bar{z} = z\nu_{mp}/R_N$, $\bar{\omega} = \omega R_N/c\nu_{mp}$, $\bar{f} = F\bar{R}f$, where R_N is an arbitrary normalization radius, the set of coupled differential equations to be solved can be rewritten as follow

$$\frac{dP}{d\varsigma} + i(\Delta - 1 + w)P = -in\frac{\bar{f}(\varsigma)w^{n-1}}{\bar{R}}, \qquad \varsigma = \frac{\beta_{\perp o}^2}{2\beta_{\|o}}\bar{\omega}\bar{z} \tag{17.a}$$

$$\theta(\varsigma_{in}) = \theta_o + q\sin\theta_o, \qquad \theta_o \text{ uniformly distributed over } [0, 2\pi] \tag{17.b}$$

$$\frac{d^2\bar{f}}{d\bar{z}^2} + \left(\bar{\omega}^2 - \frac{1}{\bar{R}^2}\right)\bar{f} = -\left(\frac{\beta_{\perp o}^2}{2\beta_{\|o}}\right)^2 I\frac{\langle P\rangle}{\bar{R}} \tag{17.c}$$

$$\bar{f}(\bar{z}_{in}) = 0, \qquad \bar{f}'(\bar{z}_{out}) = -i\left[\left(\bar{\omega}^2 - 1/\bar{R}^2\right)^{\frac{1}{2}}\bar{f}\right]_{\bar{z}=\bar{z}_{out}} \tag{17.d}$$

The problem is then completely defined by giving a resonator geometry as specified by $\bar{R} = \bar{R}(\bar{z})$ and the set of dimensionless parameters n, I, q, $\beta_{\perp o}$, $\beta_{\|o}$, Δ and $\bar{\omega}$.

The iterative procedure to solve the coupled differential equations (17) can be summarized as follows:

a) The iterations are started with $\langle P\rangle$ in the rhs of Eq.(17.c) approximated by its unperturbed values given in Eq.(12). By using the Finite Elements method[12], it can

be shown that the Eqs.(17.c,d) can be discretized into a linear system of algebraic equations. This system of equations is tridiagonal because the first order linear elements are chosen and therefore, can be solved by the very fast forward-backward substitution method[13].

b) Once the field profile $\bar{f}(\bar{z})$ is found, the equation of motion (17.a) is integrated by a first order predictor-corrector method. At the end of this step, the average complex momentum $\langle P \rangle$ as a function of $\bar{z}$ (or ς) is calculated so that the step a) can be repeated with the updated values of $\langle P \rangle$.

The iterations are performed until the efficiency $\eta_\perp$ converges to a constant value. Experience shows that 3 (for low current, low efficiency cases) up to 50 iterations are required to obtain the convergence. The accuracy of the solution is checked by computing at each iteration the error in the conservation relation (7.a). In most cases presented hereafter, relative errors less than 10^{-3} are achieved with 128 equidistant mesh point on the z-axis and 128 particles.

For low current and $n = 1$, $q = 2.0$, $\beta_{\perp o} = 0.4$, $\beta_{\perp o}/\beta_{\|o} = 2.0$, $\bar{R}(\bar{z}) = 1$ for $0 \leq \bar{z} \leq 15$, the transverse efficiency $\eta_\perp$ as a function of $\bar{\omega}$ and Δ, calculated with the procedure described above, are compared with the analytical result, Eq.(14). Figure 2 shows such a comparison for $I = 10^{-3}$. The optimum efficiency obtained numerically is 3.45% at $\bar{\omega} = 1.0070$, $\Delta = 0.054$ while the small signal model yields an optimum $\eta_\perp$ equal to 3.75% at $\bar{\omega} = 1.0064$, $\Delta = 0$. For normalized currents lower than 10^{-3}, the agreement becomes indeed better.

Increasing the current I yields a larger transverse efficiency as shown in Fig.(3) where $I = 0.075$ with the other parameters being the same as in Fig.(2). Both the optimum magnetic detuning parameter and the optimum frequency of oscillation increase ($\Delta_{opt} =$

0.86, $\bar{\omega} = 1.0232$) with an optimum efficiency equal to 66.8%. Figure 3 also shows that for each frequency, the efficiency can be optimized by adjusting Δ (i.e. the magnetic field). As a result, the bandwidth remains almost the same as in the low current case.

The field profiles for $I = 0.001$ and $I = 0.075$ are shown in Fig.(4) as a function of $\bar{z}$. The presence of a backwards wave can be noticed by examining the field amplitude in the high current case, near the end of the interaction region. Agreement between the complex field obtained here and the analytical expression given in Eq.(13) is good for the low current case.

The optimum efficiency as well as the parameters for obtaining this optimum are plotted as functions of the dimensionless current I in Fig.(5.a) and the normalized interaction length $\nu_{mp}L/R \simeq 2\pi L/\lambda$ in Fig.(5.b). Comparisons of these optimum characteristics with the results calculated by assuming a Gaussian field profile[7] show a qualitatively good agreement, as have been already found in the low field, low current case, in section III.

As a final remark, we should note that the present numerical code can be employed to analyze more realistic gyroklystrons or gyrotwystrons ($\bar{R} = \bar{R}(z)$, $\Delta = \Delta(z)$). Furthermore, a more sophisticated description of the prebunched beam at the entrance of the resonator than the simple model implied by Eq.(10) can be implemented in a straightforward manner to the present version of the code.

V. CONCLUSION

In this paper, we have made use of the self consistent equations to investigate in detail the steady state of the energy extraction stage of a gyrotwystron. In order to gain some physical insights, we have derived analytically the self consistent field profile [Eq.(13)] as well as the transverse efficiency [Eq.(14)] in the small signal regime (low field, low current). To our knowledge, these are the first analytic results for the self consistent field structure and efficiency of a gyrotron device. These results can also be used to test nonlinear numerical codes. In the large signal regime, we have employed the finite element method to solve the nonlinear self consistent field equation (section IV). Inspection of the results shows that the self consistent model and the fixed field model (Gaussian profile) yield qualitatively the same results at optimum operating conditions.

Finally, some extensions (more sophisticated initial conditions for the prebunched electron beam, introduction of velicity spread) to our numerical procedure can be worked out with modest efforts. The resulting code should be very useful for the design study of any multiple cavity gyrotrons.

ACKNOWLEDGEMENTS

This work was supported by the U.S. Department of Energy Contract No. DE-AC02-78ET51013 and in part by the Office of Naval Research. One of the authors (T.M.T.) would like to acknowledge the support received from the Swiss National Science Foundation.

REFERENCES

[1] R. S. Symons and H. R. Jory, in *Advances in Electronics and Electron Physics*, edited by C. Marton (Academic Press, New York, 1979) vol. 1, pp. 1–54.

[2] K. R. Chu, V. L. Granatstein, P. E. Latham, W. Lawson and C. D. Striffler, to be published in *IEEE Trans. Plasma Science*, 1985.

[3] A. M. Bhanji, D. J. Hoppe and R. Cormier, *Conference Digest, International Radar Conference*, Washington D.C., 1985.

[4] V. A. Flyagin, A. V. Gaponov, M. I. Petelin and V. K. Yulpatov, *IEEE Trans. Microwave Theory and Tech*, **MTT-25**, 514(1977).

[5] A. K. Ganguly and K. R. Chu, *Int. J. Electron.* **51**, 503(1981).

[6] V. S. Ergakov, M. A. Moiseev and R. É. Érm, *Radiophys. Quantum Electron.* **22**, 700(1979).

[7] T. M. Tran, B. G. Danly, K. E. Kreischer, J. B. Schutkeker and R. J. Temkin, submitted to*Phys. Fluids*, 1985.

[8] V. L. Bratman, M. A. Moiseev, M. I. Petelin and R. É. Érm, *Radiophys. Quantum Electron.* **16**, 474(1973).

[9] A. W. Fliflet, M. E. Read, K. R. Chu, and R. Seeley, *Int. J. Electron.* **53**, 505(1982).

[10] M. Caplan, *Conference Digest, Eighth International Conference on Infrared and Millimeter Waves, Florida, 1983*, (The Institute of Electrical and Electronics Engineers, New-York, 1983) paper W4.2.

[11] A. K. Ganguly and A. W. Fliflet, *Conference Digest, Ninth International Conference on Infrared and Millimeter Waves, Takarazuka, 1984*, (The Institute of Electrical and

Electronics Engineers, New-York, 1984), p. 227.

[12] G. Strang and G. J. Fix, *An Analysis of the Finite Element Method* (Prentice-Hall, Englewood Cliffs, N.J., 1973).

[13] R. D. Richtmyer and K. W. Morton, *Difference Methods for Initial Value Problems* (2nd. edition, Wiley Interscience Publishers, N.Y., 1967).

FIGURE CAPTIONS

Figure 1 Contour levels for the function $G(x, y)$ defined in Eq.(14).

Figure 2 Comparison between the numerically computed efficiency (solid line) and the analytical result given by Eq.(14) (dashed line) for $I = 0.001$, $\nu_{mp}L/R = 15$, $q = 2$, $\beta_{\perp o} = 0.4$, $\beta_{\perp o}/\beta_{\|o} = 2$, at the fundamental cyclotron harmonics. The cross near the $\bar{\omega}$-axis designates the position where the numerically computed efficiency is maximum. The contour lines show the efficiency decrease from this maximum at the rate of -1dB.

Figure 3 Transverse efficiency contour levels for the same parameters as in Fig.(2) except that $I = 0.075$. Note that the position of the maximum efficiency is now shifted to $\Delta = 0.86$, $\bar{\omega} = 1.0232$. The maximum efficiency here is equal to 0.668.

Figure 4 The rf field profile for $I = 0.001$ and $I = 0.075$ versus the normalized axial coordinate $\bar{z} = \nu_{mp}z/R$.

Figure 5 The optimum efficiency $\eta_{\perp}$, magnetic detuning parameter Δ, rf field magnitude F, oscillation frequency $\bar{\omega}$ versus (a) the dimensionless current I and versus (b) the normalized interaction length $\nu_{mp}L/R$.

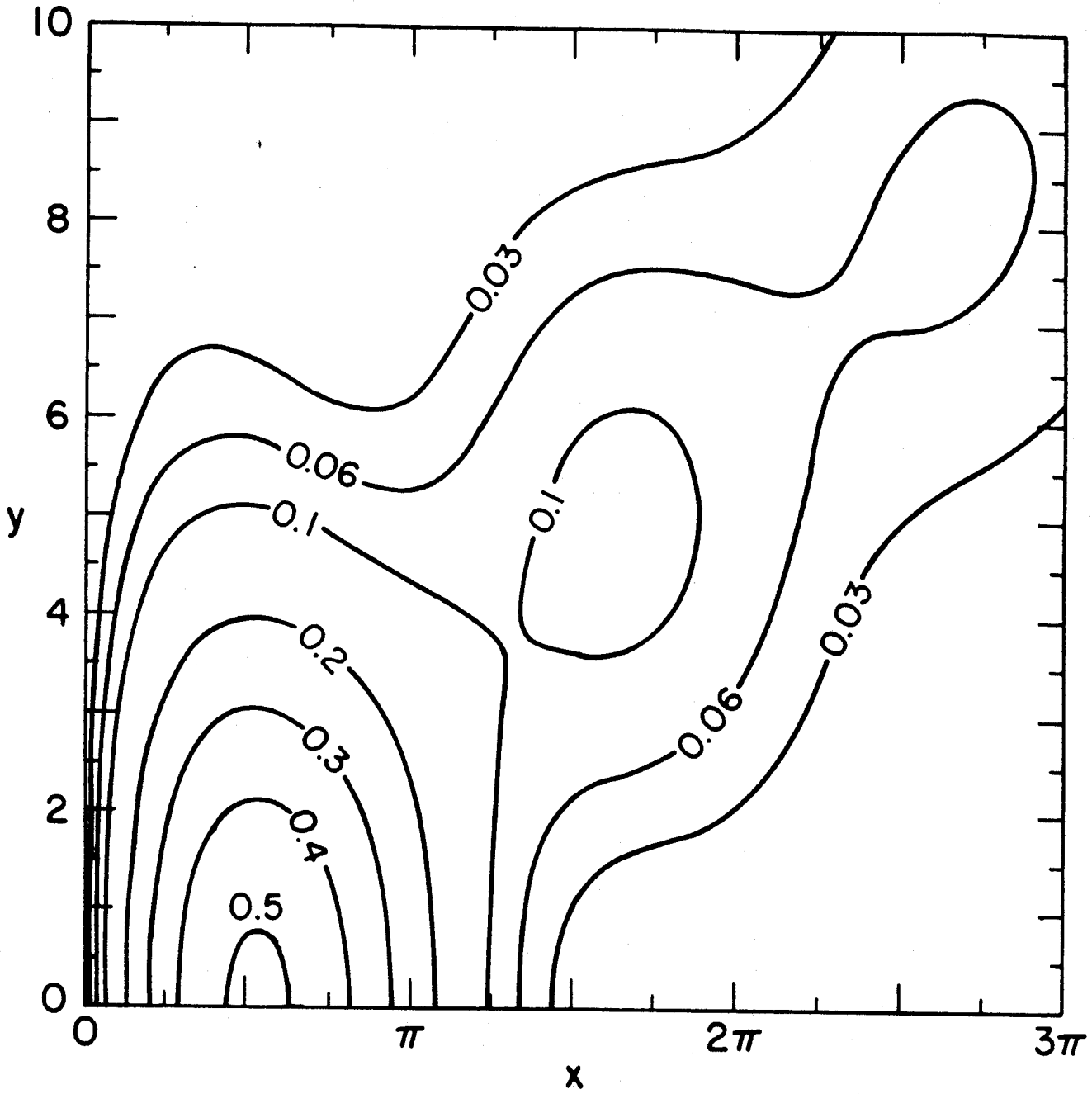

Figure 1

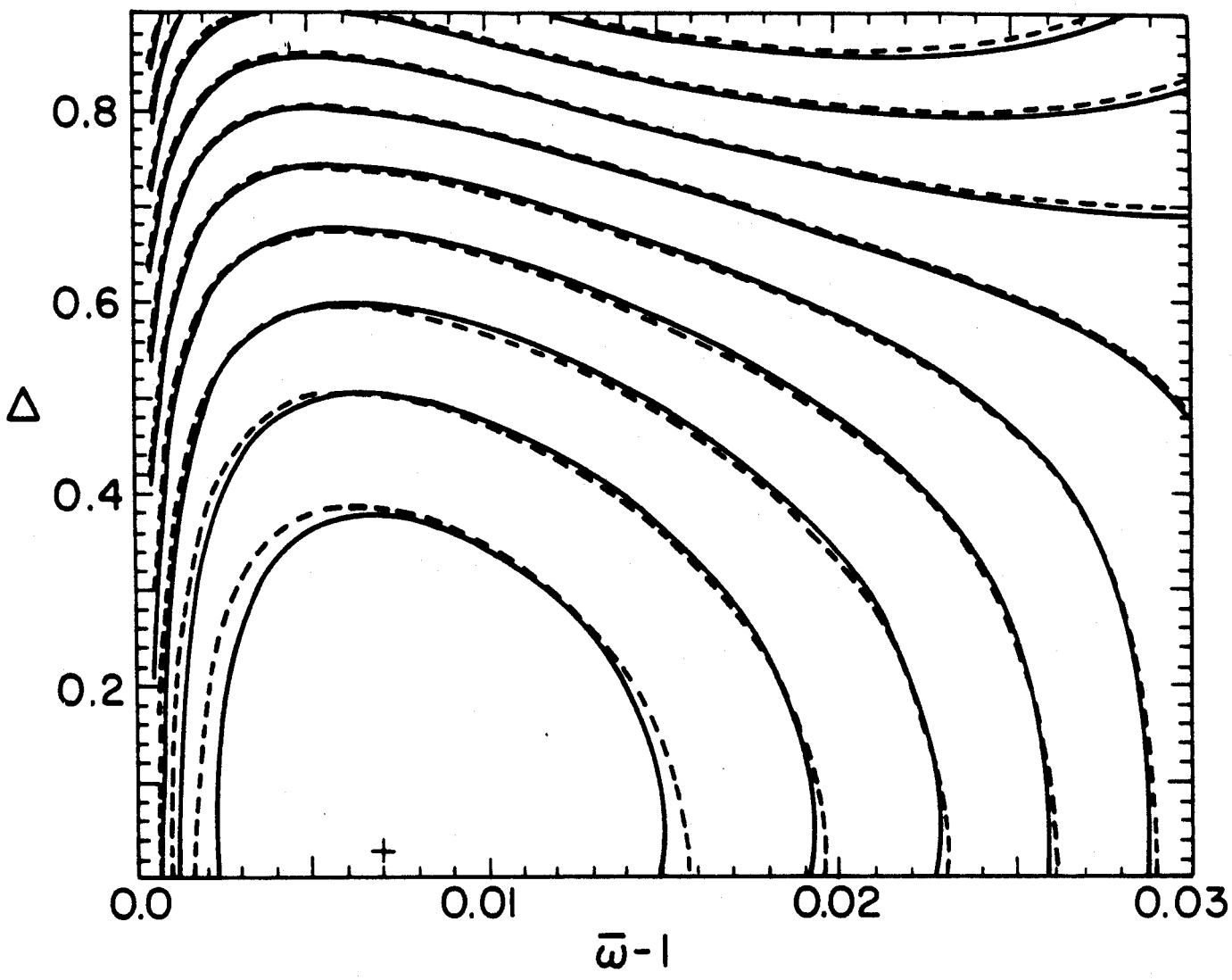

Figure 2

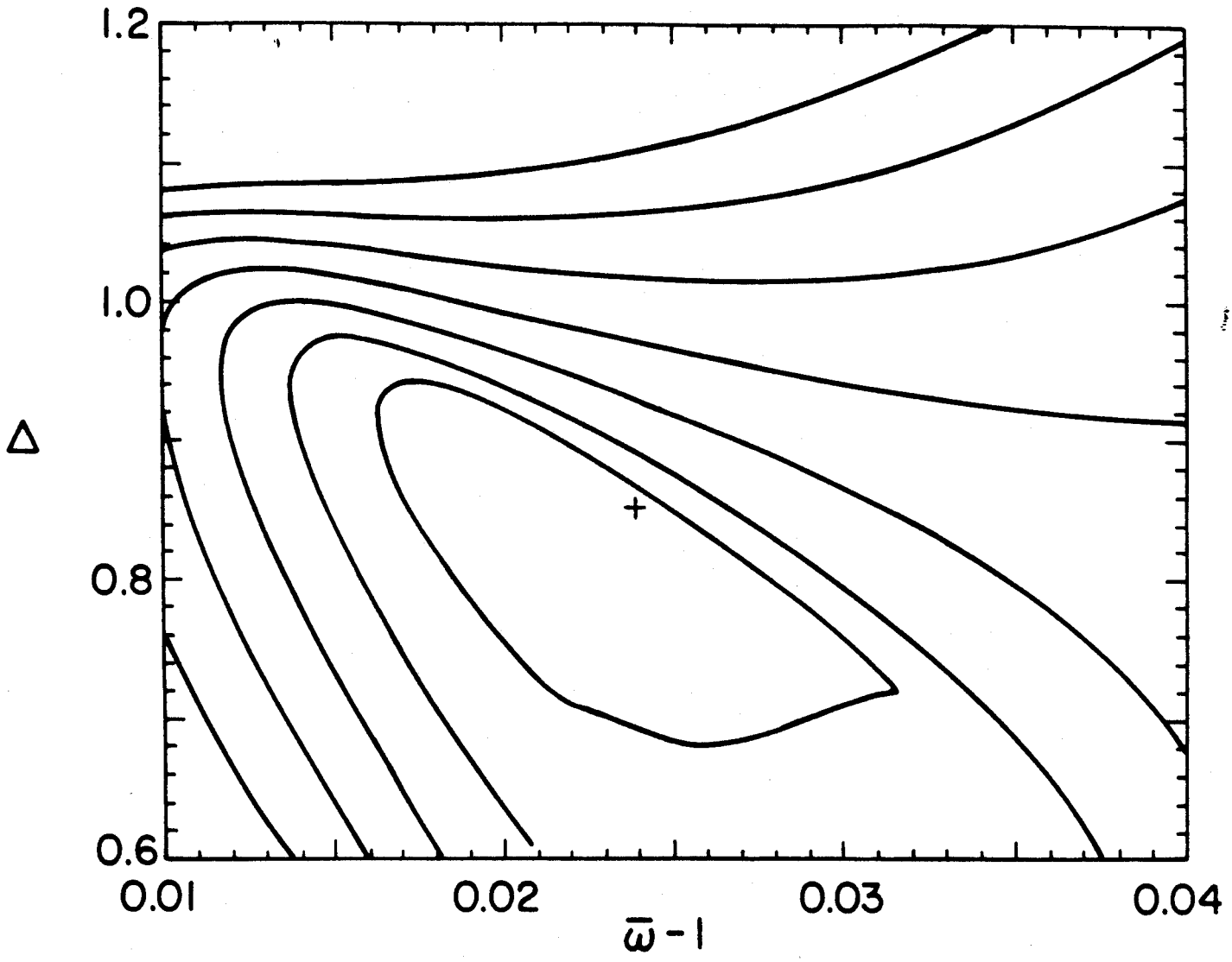

Figure 3

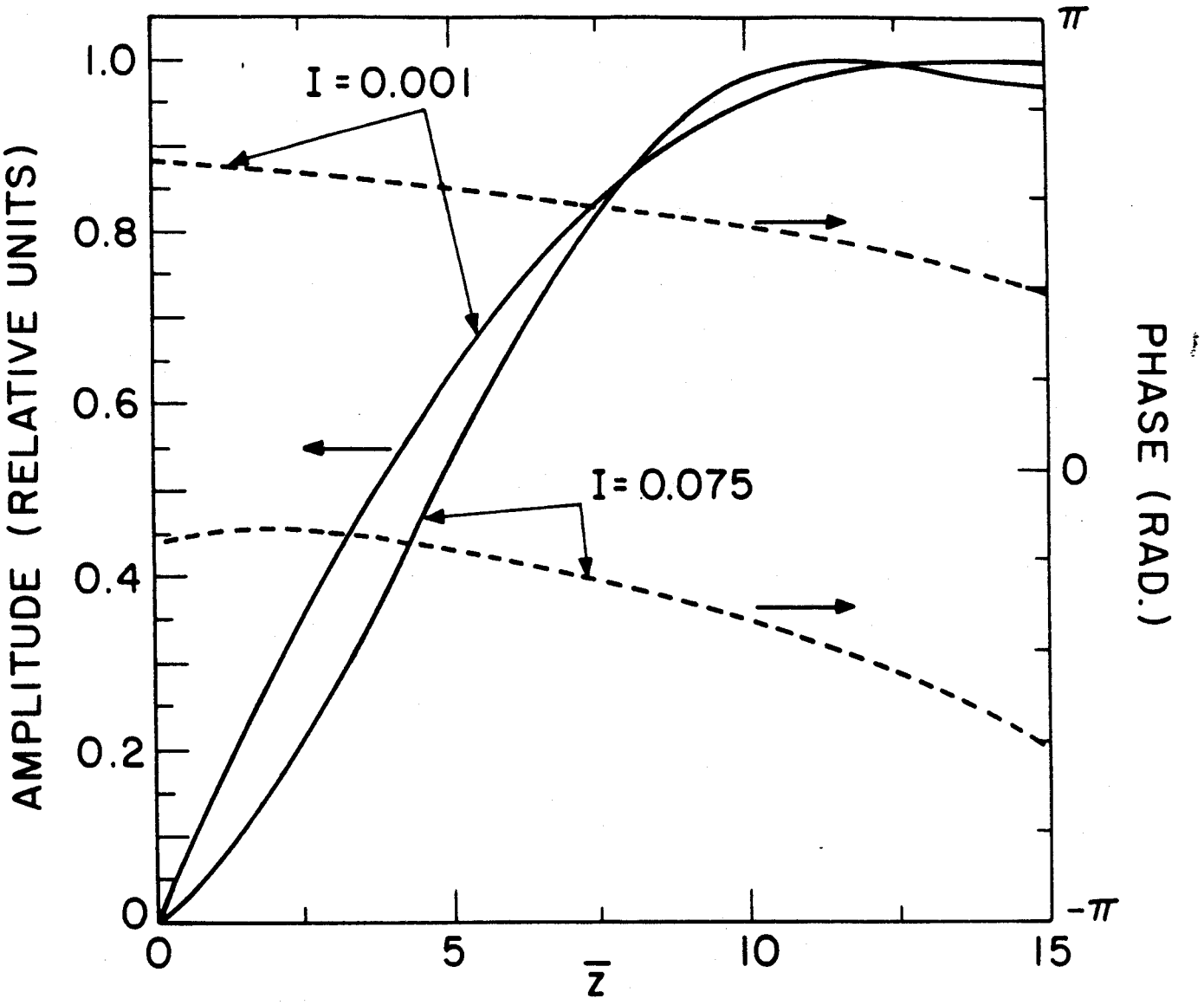
AMPLITUDE (RELATIVE UNITS)
PHASE (RAD.)
I = 0.001
I = 0.075
1.0
0.8
0.6
0.4
0.2
0
π
0
-π
0
5
10
15
z̄

Figure 4

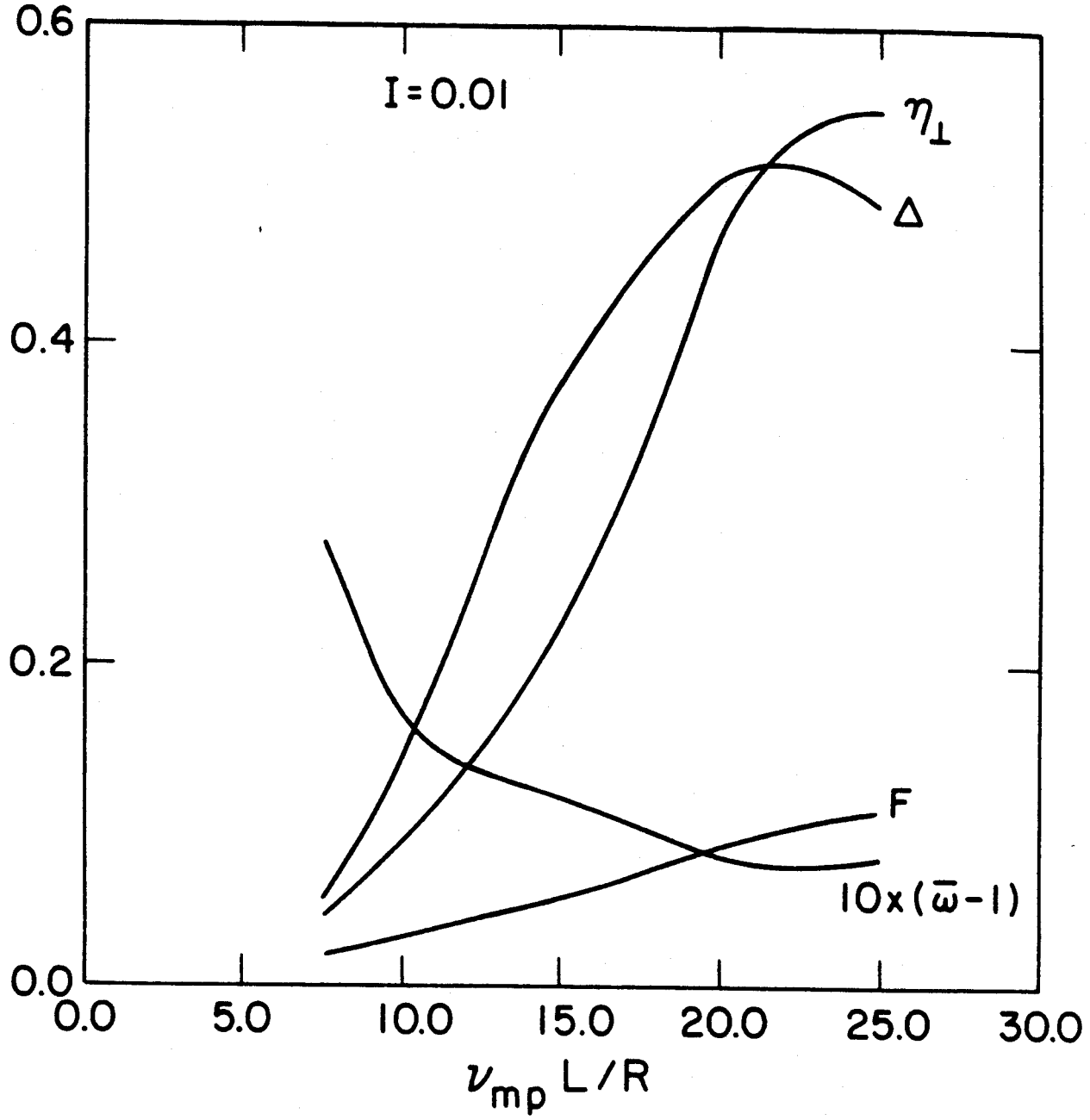
0.6
0.4
0.2
0.0
I=0.01
$\eta_\perp$
Δ
F
10x($\bar{\omega}$-1)
0.0
5.0
10.0
15.0
20.0
25.0
30.0
ν_{mp} L/R

Figure (5.a)

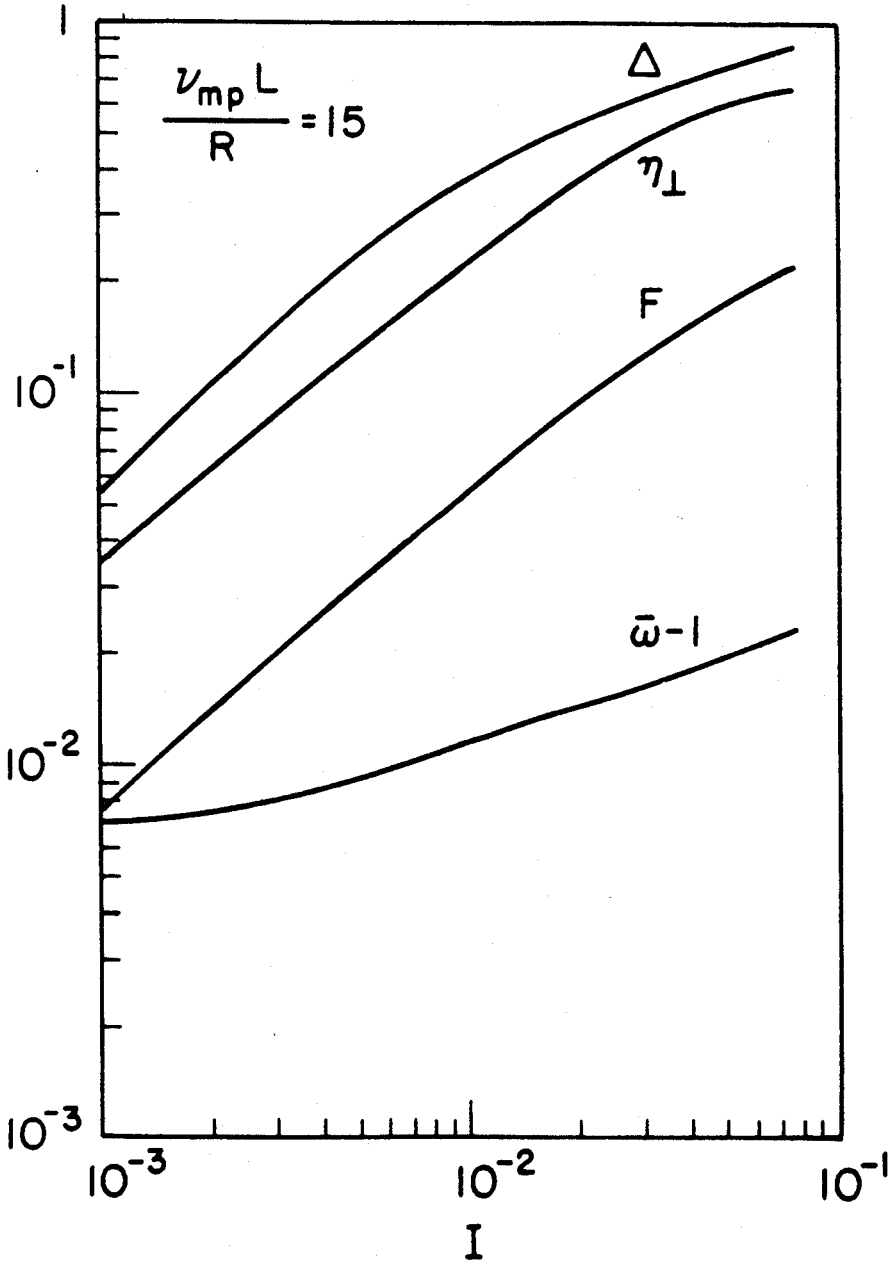
1
$\frac{\nu_{mp} L}{R} = 15$
Δ
$\eta_\perp$
F
$\bar{\omega}-1$
10^{-1}
10^{-2}
10^{-3}
10^{-3}
10^{-2}
10^{-1}
I

Figure (5.b)